Procds. of the 16th Asian Regional Conference on Soil Mechanics and Geotechnical Engineering,
October 14-18, 2019, Taipei, Taiwan

# Two-phase flow analysis for three-dimensional flow of LNAPL using CT image in porous material

Erika Shiota[1], T. Mukunoki[2], and Y. Miyata[3]

[1] Graduate School of Science and Technology, Kumamoto University, 1-39-2, Kurokami Chuou-ku, Kumamoto-shi 860-8555, Japan.
[2] Faculty of Advanced Science and Technology, Kumamoto University, 1-39-2, Kurokami Chuou-ku, Kumamoto-shi, 860-8555, Japan.
[3] National Defense Academy, Hashirimizu, 1-10-20, Yokosuka-shi, Kanagawa, 239-8686, Japan.

## ABSTRACT

The mechanism of soil contamination from light non-aqueous phase liquids (LNAPL) is complex because of the influence of three soil attributes: pore size, pore shape, and pore connectivity. At present, μ-focus X-ray computed tomography can be used to evaluate these parameters through image processing and numerical analysis. The Lattice Boltzmann Method can be used to define the boundary conditions for complex boundaries and pore structure. The purpose of this paper is to elucidate the mechanism of water–LNAPL flow in porous materials. From our quantitative analysis, we found that LNAPL flow behavior in soil is influenced by the pore space distribution and the aspect ratio for the flow direction.

**Keywords:** pore structure; LBM analysis; image analysis

## 1 INTRODUCTION

In the investigation of underground contamination, it is important to accurately estimate the complicated behavior of pollutants in soil. We have been investigating methods for state estimation and flow analysis for soil contamination by light non-aqueous phase liquids (LNAPL). On the contaminant state, we found that the soil pore structures could be analyzed using CT image analysis and the distribution of LNAPL in the soil. On the flow analysis, we found that the behavior of LNAPL in soil was affected by the complicated 3-D pore structure. These findings were obtained using the lattice Boltzmann method (LBM) (Mukunoki et al. 2013). In this study, we performed a 3-D two-phase flow analysis of glass beads and Toyoura sand using CT image analysis. Our results enabled the quantitative characterization of the pore structure of sand.

## 2 IMAGE AND NUMERICAL ANALYSIS(

### 2.1 Image processing

We used glass beads and Toyoura sand (average particle diameters of 350 and 250 μm, respectively) to investigate the importance of considering the complex soil pore structure in estimating LNAPL behavior. The specimens were prepared using a free fall method to obtain the prescribed porosities (36% for glass beads and 40% for Toyoura sand) in a mold with an inner diameter of 10 mm. Then the specimens were scanned by μ-CT (TOSCANNER 32300). Multiphase segmentation was applied on these images using the marker-controlled watershed method to compare the pore distribution before and after LNAPL injection. The pore distributions were evaluated quantitatively using the 3D granulometric method (3DGM) proposed by Mukunoki, et al. (2016).

### 2.2 LBM analysis for pore structure

To estimate the behavior of LNAPL in soil, it is necessary to consider the interactions of water, LNAPL, and the solid boundary. The LBM can be applied to such complicated geometries. We analyzed the 3-D two-phase flow system by LBM using the model developed by Shan and Chen (1993), which was later improved by Pan et al. (2004). This model can simulate 3-D isothermal multiphase flow. We used the results of the 3DGM in section 2.1 as input to the model. The LNAPL was injected with a constant flow volume at the boundary of the saturated specimen.

Fig. 1 shows the outline of the analysis. The orange, blue, and gray areas represent the LNAPL, solid particles and water, respectively. For the flow of water and LNAPL, bounce back boundary conditions were applied at the inlet and outlet sides of the flow domain. In the boundary condition on the other four planes, the direction parallel to the plane was set as a non-slip condition and the vertical direction was set as a periodic boundary condition. The simulation represented a two-phase flow system driven by the pressure difference between the inlet and outlet. The initial conditions included the density of LNAPL ($\rho_N$) of 100 at the inlet; at the outlet, the density ($\rho_w$) was set at 90

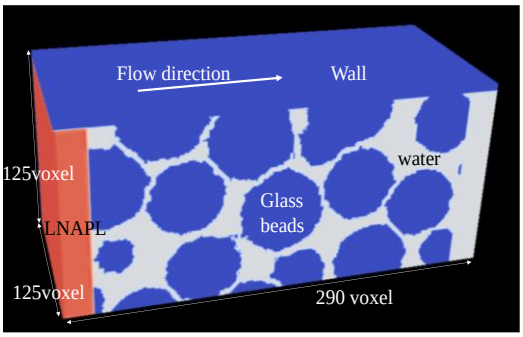


(a) Glass beads

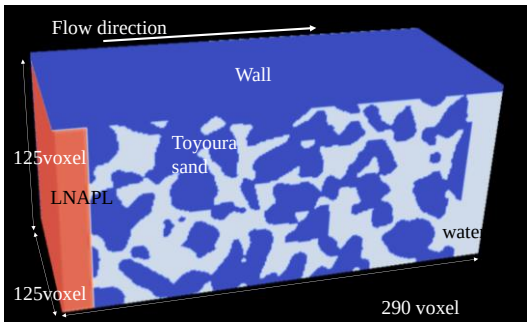


(b) Toyoura sand

Fig. 1. Initial condition of LBM for pore structure.

Table 1. Parameters using two-phase flow in 3D.

| parameters | LNAPL | Water |
|---|---|---|
| Density ratio | 1 | 1 |
| Relaxation time (τ) | 1.167 | 1 |
| Fluid – fluid Interaction ($g_f$) | 0.0015 | 0.0015 |
| Fluid – solid Interaction ($g_s$) | -0.020 | 0.020 |

for the glass beads and 80 for the Toyoura sand. Table 1 shows the other parameters used in the analysis. These values were obtained from contact angle and drop tests (Maghsoudi et al., 2018); the contact angle between the LNAPL and the solid particles was approximated at 75°.

### 2.3 LBM analysis for pipe model

To study the effect of pore connectivity in the flow direction, we created a pipe model based on the pore structure obtained from the CT image.

The pipe diameter represented the average pore size in a given space, and the flow occurred along the direction of an orthogonal axis only. Fig. 2 shows the flowchart of the modeling process. A 3-D image of the pore spaces was segmented as shown in Fig. 2 (a), and the mean pore size in each region was calculated and used as the pipe diameter in Fig. 2(b). Finally, we created a pipe model defining the flow domain as shown Fig. 2(c). The pipe model representing the pore structures of the Toyoura sand and glass beads was applied in the 3-D two-phase flow analysis of the interaction between water and LNAPL. The analysis domain was 240 voxels in width, 125 voxels in height, and 125 voxels in depth. The density of LNAPL ($\rho_N$) was set at 100 at the inlet for both materials; at the outlet, the density ($\rho_w$) was set at 85 for the glass beads and 70 for the Toyoura

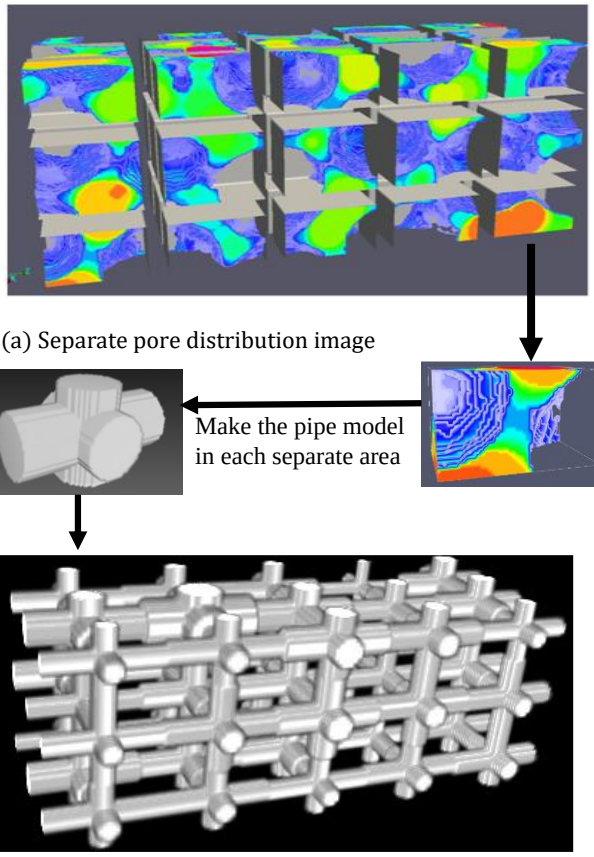


(a) Separate pore distribution image

(b) Schematic of pipe model

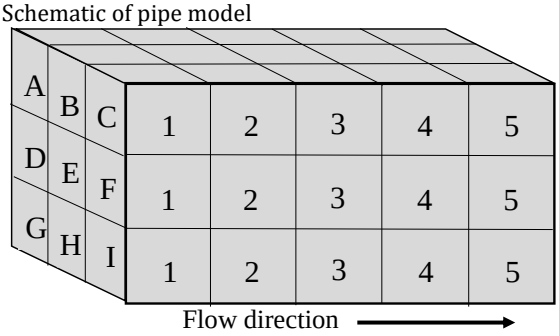


(c) Definition of pipe model area

Fig. 2. Process of making pipe model.

sand. The remaining boundary conditions were the same as those defined in section 2.2.

## 3 RESULTS OF ANALYSIS

### 3.1 Analysis of pore structure

Fig. 3 shows the pore structures of both materials based on the 3DGM results. The color contours indicate the pore sizes. Based on these results, the pore size distributions and histograms of injected LNAPL in the pores of the glass beads and Toyoura sand are shown in Fig. 4. The total number of voxels for the whole domain normalized the number of voxels for the entire pore and the pore space occupied by LNAPL. In all samples, LNAPL is distributed across the entire pore area; however, the average pore diameter occupied by LNAPL tends to be slightly larger than the total pore

diameter.

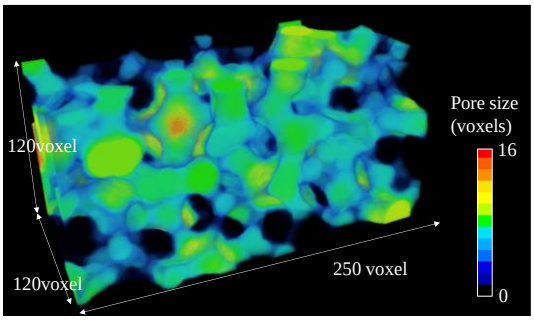


(a) Glass beads

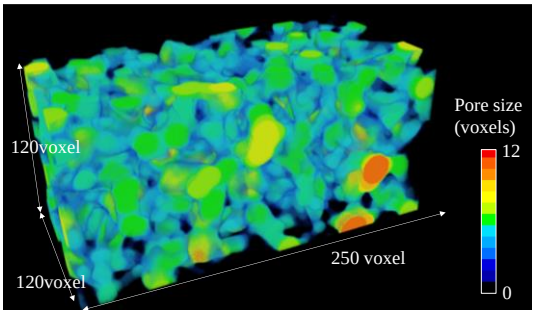


(b) Toyoura sand

Fig. 3. Pore structures from results of 3DGM.

### 3.2 Results of LBM for pore structure

Fig. 5 shows the LNAPL distribution obtained from the LBM analysis of the pore structures of the glass beads and Toyoura sand at the last time step of the simulation. These diagrams illustrate the LNAPL distribution for flow paths starting from the left side and reaching the right side. In both cases, LNAPL is observed quantitatively in the flow paths. Comparing this result with those in Fig 4 and the results of the 3DGM for the percolated LNAPL, it was noted that LNAPL preferred the larger pore spaces for the glass beads and Toyoura sand specimens.

### 3.3 Result of LBM analysis for pipe models

Fig. 6 shows the results of the LNAPL flow analysis using the pipe models. It was noted that substantial flow occurred in certain regions and along certain paths. The flow distribution shown in Fig. 7 indicates that LNAPL flow occurred in every region of the flow domain. For the glass beads, the area with the highest LNAPL flow was area F. For Toyoura sand, the highest LNAPL flow occurred in areas B, C, E, I. In the next section, we evaluate the spatial distribution pores in the pipe model.

### 3.4 Quantification of pore structure for flow direction

The average pore diameter (APD) in the 45 regions along the flow direction shown in Fig. 2(c) was defined as follows (assuming the vertical areas A–I and the horizontal areas 1–5 in the flow direction):

$$\mathrm{APD} = \frac{\sum_{n=1}^{5} D_n}{5} \qquad (1)$$

where $D$ is the pore diameter in each area (A–I). Then,

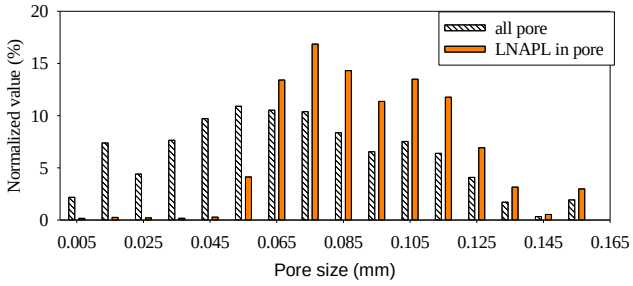


(a) Glass beads

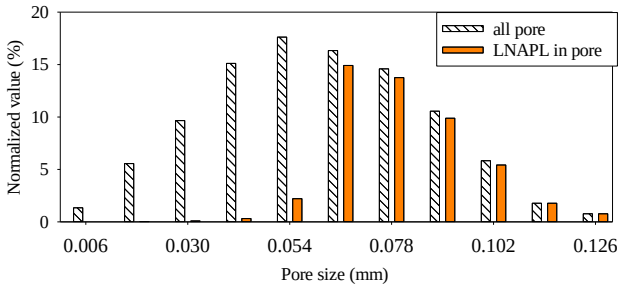


(b) Toyoura sand

Fig.4. Histogram of pore distribution.

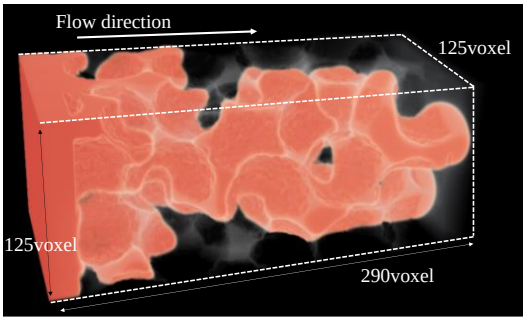


(a) Glass beads

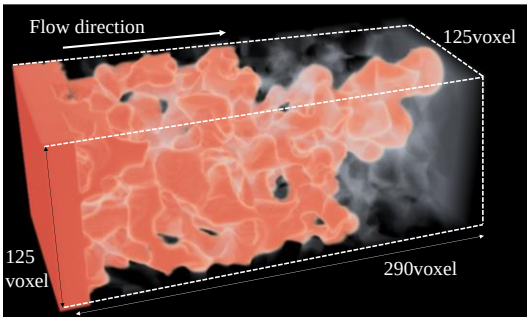


(b) Toyoura sand

Fig.5. Result of LBM for pore structure.

the average aspect ratio (AAR) was defined as an index showing the change in pore diameter.

$$\mathrm{AAR} = \frac{\sum_{n=1}^{4} |D_{n+1} - D_n|}{4} \qquad (2)$$

When the pore is equal to the next pore size in the flow direction, AAR is zero. The larger the change in pore diameter of each area, the larger is the AAR in the flow direction. We propose four pore structure patterns based on APD and AAR. Fig. 8(a) and (b)show the

relation between APD and AAR for areas A–I, and the

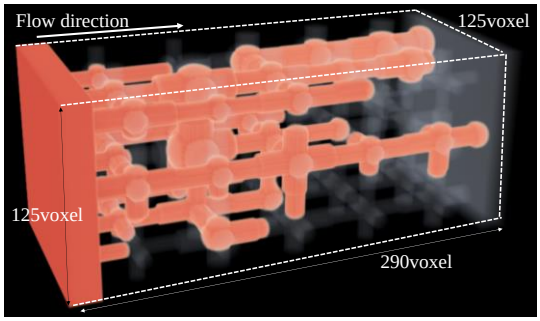


(a) Glass beads

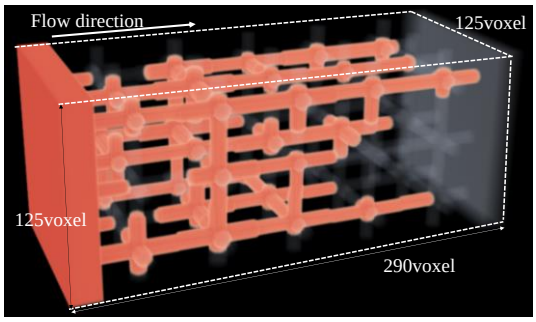


(b) Toyoura sand

Fig. 6. Result of LBM for pipe model.

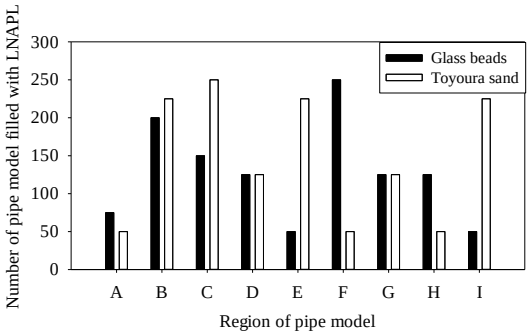


Fig. 7. Flow distance of LNAPL for each area.

pore structure patterns are grouped into four categories (a, b, c, and d) based on the total APD and total AAR.

For the glass beads (Fig.8(a)), it was noted in area F, which has the highest flow (Fig. 7), that the pore diameter was smaller than the APD, and the aspect ratio was larger than the AAR. However, LNAPL flow is difficult in the area A under conditions defined by the category a, which is symmetric relation with category d. For Toyoura sand (Fig. 8 (b)), it was noted that the areas B, C, E, and I, which convey the highest LNAPL flows (Fig. 7), are defined by pore structures within or near category d. Therefore, these results show that the preferential flow path for LNAPL tends to occur through pores that are larger than the APD.

## 4 CONCLUSION

In this study, we analyzed μX-ray CT images for glass beads and Toyoura sand, specimens that are uniform particles. We discussed the results of a 3-D two-phase flow simulation for LNAPL using the 3-D pore distribution obtained from the LBM analysis. We

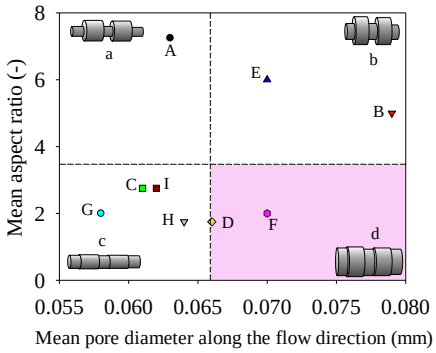


(a) Glass beads

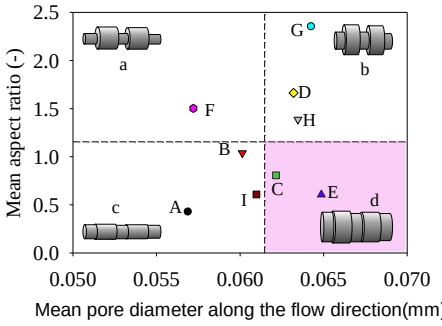


(b) Toyoura sand

Fig. 8. Relation between APD and AAR. Short dashes lines mean the total APD and total AAR.

analyzed the LNAPL flow behavior and replace the complicated pore structure with a pipe model. From our quantitative analysis, we also found that LNAPL flow behavior in soil is influenced by the pore space distribution and the aspect ratio for the flow direction.

## ACKNOWLEDGEMENTS

This research was financially supported by JSPS Research fellow (17J11642). Authors thanks to Ms. Chiaki Nagai, from to Maeda Corporation.

## REFERENCES

Shan, X., & Chen, H. (1993). Lattice Boltzmann model for simulating flows with multi phases and components. *Physical Review E*, *47*(3), 1815–1819. https://doi.org/10.1103/PhysRevE.47.1815

Pan, C., Hilpert, M., & Miller, C. T. (2004). Lattice-Boltzmann simulation of two-phase flow in porous media. *Water Resources Research*, *40*(1), 1–14. https://doi.org/10.1029/2003WR002120

Mukunoki, T., Nagai, C., Fujiki, Y., & Mikami, K. (2013). Evaluation of oil contamination in porous media by X-ray CT image analysis and LBM simulation. In *7th International Joint Symposium on Problematic Soils and Environment in Asia*, 63–66. Okinawa, Japan.

Mukunoki, T., Miyata, Y., Mikami, K., & Shiota, E. (2016). X-ray CT analysis of pore structure in sand. *Solid Earth*, *7*(3), 929-942. https://doi.org/10.5194/se-7-929-2016

Maghsoudi, K., Momen, G., Jafari, R., & Farzaneh, M. (2018). Direct replication of micro-nanostructures in the fabrication of superhydrophobic silicone rubber surfaces by compression molding. *Applied Surface Science*, *458*(July), 619–628.

https://doi.org/10.1016/j.apsusc.2018.07.099